Grid capacity and efficiency enhancement by operating medium voltage AC cables as DC links with modular multilevel converters

Shekhar, Aditya; Kontos, Epameinondas; Ramírez-Elizondo, Laura; Rodrigo-Mor, Armando; Bauer, Pavol

DOI
10.1016/j.ijepes.2017.06.012

Publication date
2017

Document Version
Final published version

Published in
International Journal of Electrical Power & Energy Systems

Electrical Power and Energy Systems 93 (2017) 479–493

Contents lists available at ScienceDirect

Electrical Power and Energy Systems

journal homepage: www.elsevier.com/locate/ijepes

Grid capacity and efficiency enhancement by operating medium voltage AC cables as DC links with modular multilevel converters

Aditya Shekhar *, Epameinondas Kontos, Laura Ramírez-Elizondo, Armando Rodrigo-Mor, Pavol Bauer

Delft University of Technology, Building 36, Mekelweg 4, 2628CD Delft, The Netherlands

ARTICLE INFO

Article history:
Received 12 September 2016
Received in revised form 22 April 2017
Accepted 9 June 2017
Available online 26 June 2017

Keywords:
Capacity
Dc links
Cables
Distribution
Dynamic rating
Efficiency
Electric fields
Grid
Medium voltage
MMC
Payback

ABSTRACT

It is anticipated that with the thrust towards use of clean energy resources such as electric vehicles, future distribution grids will face a steep increase in power demand, forcing the utility operators to invest in enhancing the power delivering capacity of the grid infrastructure. It is identified that the critical 5–20 km medium voltage (MV) underground ac distribution cable link, responsible for bulk power delivery to the inner urban city substation, can benefit the most with capacity and efficiency enhancement, if the existing infrastructure is reused and operated under dc. Quantification of the same is offered in this paper by incorporating all influencing factors like voltage regulation, dc voltage rating enhancement, capacitive leakage currents, skin and magnetic proximity effect, thermal proximity effect and load power factor. Results are presented for three different ac and dc system topologies for varying cable lengths and conductor cross-sections. The computed system efficiency is enhanced with use of modular multilevel converters that have lower losses due to lower switching frequency. A justified expectation of 50–60% capacity gains is proved along with a generalized insight on its variations that can be extrapolated for different network parameters and configurations. Conditions for achieving payback time of 5 years or lower due to energy savings are identified, while the socio-economic benefits of avoiding digging and installing new cable infrastructure are highlighted. The technical implications of refurbishing cables designed for ac to operate under dc conditions is discussed in terms of imposed electric fields, thermal profile and lifetime. A novel opportunity of temperature dependent dynamic dc voltage rating to achieve additional capacity and efficiency gains is presented.

1. Introduction

Fueled by the thrust for green energy resources, proliferation of new energy consumers like electric vehicles (EV), all electric houses and heat pumps has changed the localized energy consumption patterns and increased the expected power demand from grid infrastructure [1,2]. Charging modern electric cars at once during a specific time of the day may induce temporary and localized power deficits [3,4]. With emerging concepts of electric houses and heat pumps, the demand is expected to increase significantly [5,6].

1.1. Concept description and application

The forecasted increase in demand is anticipated to force the utility operators to enhance the power delivery capacity of their distribution networks. For example, recently an all electric bus fleet was deployed in Amsterdam, making its international airport one of the largest e-bus charging stations in Europe [7]. Similarly, an electric bus fleet with on-road charging solution is planned in the Province of North Holland [8]. While the radial links from the city central substation to the local pocket of increased power demand may be of adequate capacity, the medium voltage link bringing bulk power from the outskirts, as shown in Fig. 1, may need expansion.

The straightforward option available is to install new ac grid infrastructure along with additional cable links. However, this approach will not only result in high incurred costs and occupied space, but also involve a massive digging and installation operation which is not always practically feasible. With expensive digging, particularly in old heritage cities of countries such as Netherlands, socio-economically viable solutions to address localized power deficits are of urgent need.

In this context, it is proposed to refurbish the existing ac underground cable to operate under dc conditions to achieve enhancement in power transfer capacity [9]. The potential of capacity enhancement with dc operation has been previously stressed

* Corresponding author.
E-mail address: a.shekhar@tudelft.nl (A. Shekhar).

http://dx.doi.org/10.1016/j.ijepes.2017.06.012
0142-0615/

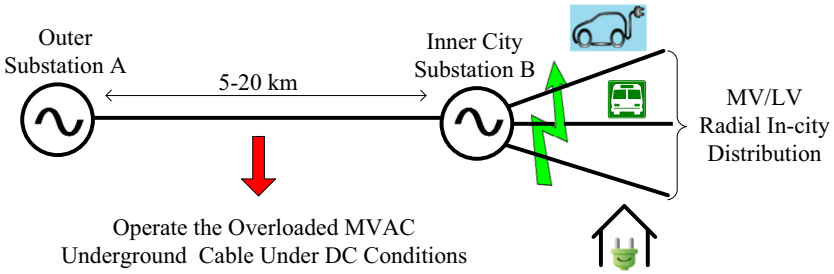

Fig. 1. Reconfigurable DC links for bulk power transmission into the city collection centre.

[10,11]. Furthermore, most of the transmission losses in the distribution grid occur in these first few kilometres of cables, and hence employing dc links for efficiency enhancement at these locations would be beneficial.

1.2. Capacity enhancement claims and state of the art

While the delivered power can be enhanced with dc, different claims on the factor by which it is increased exist in the literature. For instance, an early work illustrates that an increase of 3.5 times is feasible [12] for overhead lines. The assumption here is that a single HVDC pole voltage could be raised to twice the line to line rms ac voltage. Clearly, this may not be possible for underground cables due to insulation constraints. Furthermore, a closer scrutiny shows that the capacity gains were achieved by changing the tower head, insulator assemblies and configuration. Though it is true that maximum ac voltage is limited by distance and stability issues, it is unclear how much of the reported gains are achieved solely due the use of dc, and how much because the voltage itself was raised.

Another study [13] takes this into account and proposes a combined ac-dc operation of the same conductor without exceeding the peak of the phase rms voltage V_{ph}. Here, a dc component of $V_{ph}/\sqrt{2}$ was superimposed on the ac of $V_{ph}/2$. The reason a complete changeover to dc operation was not considered was to avoid a dc circuit breaker. But for point to point connections, the ac breaker could be on the ac side of the link, and therefore, this operationally and infra-structurally complex composite ac-dc operation can be avoided. A capacity gain of 75–85% was reported as the power angle varied from 30° to 80°. This idea was proposed for extremely high voltage long distance overhead lines, wherein, the capacity gains were due to dynamic stability constraint that did not allow for the loading of purely ac transmission to its thermal limit. This may not be a critical constraint at medium voltage short distance underground cables that we are considering.

A more recent work by Larruskain [14,15] looks into converting high voltage ac overhead lines and describes a capacity increase of 150% (factor of 2.5) by choosing a more careful voltage enhancement factor. Nevertheless, in case of underground cables, even more care must be taken, keeping in mind the insulation performance. Moreover, the purpose of their study was to offer approximate numbers for specific cases, representing order of magnitude of power increase and loss reduction [14]. Simplifying assumptions such as 5% voltage drop and 5% current enhancement were helpful to gather sense of the potential of this concept with some test cases. However, trends pertaining to varying conductor area and receiving end load power factor were not explored. For instance, the voltage drop is more prominent for lower conductor cross-sections and varies with load power factor, while the current enhancement is greater for higher area of cross sections. Furthermore, capacitive currents and dielectric losses also play a role in cables, unlike overhead lines.

Therefore, need was felt to derive a mathematically meticulous, generalized understanding of capacity enhancement adapted for refurbishing underground cable infrastructure. The mathematical framework, developed in Appendix A was derived by the authors to help take into account the exact contributions of all influencing factors. Trends associated with varying parameters will help future utility operators to decide whether it is beneficial to refurbish their system from ac to dc operation. The authors show that at least 50% capacity enhancement (factor of 1.5) is possible, thereafter varying with different factors.

1.3. Choice of dc link converter

For short distance (5–20 km) medium voltage operation, the efficiency gains of dc cable operation is significantly offset by the converter losses. The economic payback of the small system efficiency enhancement has a trade-off with costs of the converter station. Further, at medium voltage grid level, the operation should have flexibility to provide different ancillary services with minimal harmonic distortion or need for filters. Multi-level Modular Converters (MMC) offer a solution which has recently been widely used in HVDC transmission projects due to its inherent characteristics of control flexibility, low harmonic distortion on the ac current and voltage and low converter losses amongst others [16]. Therefore, the present study considers the use of MMC as a building block for the dc link.

Modularity is perhaps a more important reason for our choice because the grid location of this application is a critical link responsible for powering the city centre. In case of sub-module faults, the ability to bypass the malfunctioning converter section is desirable. Apart from this redundancy, it is vital for the novel concept of "dynamic voltage rating" we propose in this paper.

1.4. Research focus and contributions

In Section 2, the meticulous mathematical quantification of transferred power capacity enhancement is offered. Herein, the influence of different factors like voltage regulation, dc voltage rating enhancement, capacitive leakage currents to ground, skin and magnetic proximity effect, thermal proximity effect and load power factor towards reduction in delivered receiving end power is taken into account. The derived equations to incorporate all these effects are detailed in Appendix A. Different cases of the system topology of the existing ac infrastructure and the final dc link topology are explored and the variation in capacity enhancement with different cable lengths and conductor cross-sectional areas is discussed to provide a generalized understanding of the possibilities offered by the proposed concept. Realistically, 50–60% of capacity enhancement was found to be achievable.

Section 3 develops a quantified insight into the system level efficiency by computing the energy savings due to efficient dc operation of the medium voltage underground cables and

subtracting the converter losses that are incurred in the MMC stations at both the ends. The trade off of the proposed concept is higher investment cost with converter stations, which is taken into account to compute the payback time. About 5 years payback was found to be realistic to achieve in specific topologies while it was even lower for cables of lower cross-sectional areas.

Section 4 highlights the technical considerations and challenges in reusing and operating the existing ac cables under dc conditions in terms of imposed electric fields, thermal degradation of the insulation and lifetime degradation due to growth of defects at medium voltage levels. A novel opportunity of temperature dependent dynamic voltage rating of the cable is presented and its advantage in additional capacity and efficiency gains is discussed.

Finally, Section 5 concludes the key findings of the study and provides the readers with usable numbers for applying similar concepts in their research. The generalized insight on the capacity, efficiency and payback time variations that the main sections offer will also help to extrapolate these results to other system parameters.

2. Quantification of power transfer capacity enhancement

By refurbishing medium voltage ac cables to operate under dc conditions, capacity and efficiency enhancement can be achieved in power transferred by the link [9]. In this section, the mathematical quantification of achievable capacity and system efficiency gains is presented by considering all the contributing factors identified in [9]. The factors include voltage regulation, capacitive currents, load power factor, dielectric loss reduction, absence of skin effect and magnetic proximity, thermal proximity, imposed voltage rating enhancement and the ac to dc topology configuration. The mathematical equations derived to incorporate these factors are developed in Appendix A. 3-core 11 kV armoured XLPE insulated medium voltage cables with copper conductor of varying conductor cross-sectional areas and link length are considered for computing the results. The specifications are mentioned in Table B.2 in Appendix B.

2.1. Receiving end power for a MVAC π-cable link

In conventional network analysis and stability problems, receiving end voltage is considered as the reference phasor at rated value of 1 p.u. In order to quantify the influence of voltage regulation, capacitive currents and load power factor, it is necessary to compute the receiving end power for a MVAC π model of the cable under sending end rated voltage and current operating conditions shown in Fig. A.14 of Appendix A. In such a situation, the sending end voltage must be considered as the reference phasor, for which the network equations are not as straightforward [17].

For varying cable parameters based on the conductor area of cross-section and length, varying load power factor and the known rated reference sending end voltage phasor, power transferred to the receiving end of the cable link must be computed. In this problem, the unknown variables are the phase angle of the sending end current and the magnitude of the load impedance that would impose the rated cable current magnitude at the sending end of the link.

The mathematical expressions (1) and (2) for the unknown parameters $|Z_L|$ and θ_S are derived in Appendix A [17]. The solution for 7272 varying cable link and load power factor conditions is described with Fig. A.15.

$$|Z_L| = \frac{|V_S||D|\sin\delta - |I_S||B|\sin(\beta+\theta_S)}{|I_S||A|\sin(\theta_S+\theta_R+\alpha) - |V_S||C|\sin(\theta_R+\gamma)} \quad (1)$$

$$\theta_S = \sin^{-1}\left(\frac{\lambda}{\sqrt{x^2+y^2}}\right) - \tan^{-1}\left(\frac{y}{x}\right) \quad (2)$$

Fig. 2 depicts the receiving end real power in p.u. for varying cable lengths and conductor cross-sectional area for unity load power factor. By depicting in p.u., the increase in power due to increasing current rating is cancelled out.

The reduction in power is due to reduced voltage regulation and greater capacitive currents in the π-network. The

- The X-Z projection of power profile shows a linear decrease in the transmitted power with increasing cable length. This is because the resistance and inductance of the cable increase, leading to reduced voltage at receiving end. Also, the capacitive currents increase, leading to lower receiving end current.
- The Y-Z projection shows a non linear decrease in the transmitted power with decreasing cable conductor cross-sectional area. This variation is more significant for smaller cross-sectional areas.
  This is because as the area increases, the cable resistance and inductor decrease, leading to better voltage regulation, and hence higher p.u. transmitted power. However, the greater capacitance leads to reduction in the receiving end current, thereby reducing the power. The profile of the transmitted power with variation in conductor area is, hence, a result of these two opposing factors.
- The p.u. real power profile is shown for unity load power factor. The reduction in real power is more or less linear with decreasing load power factor for any cable length and area.

The computed receiving end transmitted ac power presented in this subsection takes into account the capacity drop of the underground link due to voltage regulation, capacitive currents and load power factor under rated operating conditions at the sending end.

2.2. DC current capacity enhancement

The magnitude of current that can flow through the cable is constrained by its thermal limit. From the context of current capacity enhancement, the cable is able to deliver more power to the receiving end of the transmission line in dc conditions as compared to operation in ac conditions based on the following aspects:

2.2.1. Dielectric loss reduction

Heating due to dielectric losses becomes important when the cable is operating near its thermal limit, thereby limiting the current rating of the cable [18]. With ageing, these losses can increase and further deteriorate the insulation lifetime. Under dc operating

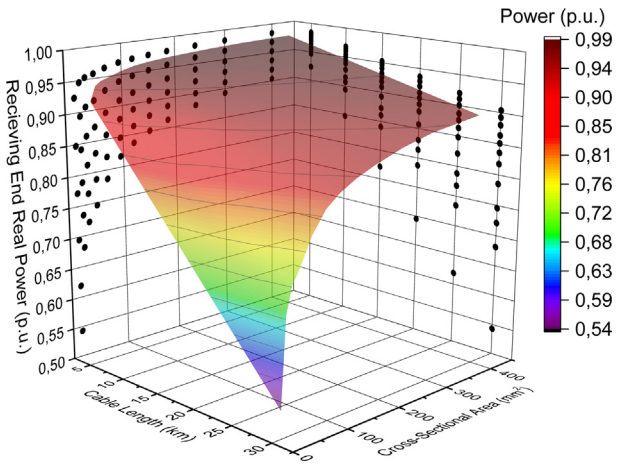

Fig. 2. Variation in receiving end transmitted real power with cable length and conductor cross-sectional area at unity load power factor.

conditions, the leakage losses through the insulation resistance are still present. However, the dipole losses due to ac electric fields are absent. The dielectric losses under ac and dc conditions are given by (3) and (4), respectively.

$$P_{\text{loss,ac}} = V^2_{\text{ac,rated}}(C_{\text{ph}}\omega)\tan(\delta) \tag{3}$$

$$P_{\text{loss,dc}} = \frac{\sqrt{2}V^2_{\text{ac,rated}}(2\pi r)}{\rho_{\text{ins}}} \tag{4}$$

Herein, the ac dielectric loss dissipation factor ($\tan(\delta)$) for XLPE medium voltage cable is taken as 10^{-4} [19–21]. Under dc conditions, the dielectric losses are without the dipole losses and only include those due to the leakage current through the insulation with resistivity (ρ_{ins}) taken as 10^{15} Ω-m [22,23]. The rated cable voltage under dc operating condition is considered to be $\sqrt{2}V_{\text{ac,rated}}$, which will be justified in Section 2.3.2.

For the 12 cables of different area of cross-section considered in this work and described in Appendix B, the losses under dc conditions is only 0.0003–0.0005% of the ac dielectric losses. However, considering that the ac dielectric losses are less than 0.01% of the ac conduction losses, their contribution in capacity and efficiency enhancement under dc operating conditions is marginal.

2.2.2. Absence of skin & magnetic proximity effect

Skin and proximity effect in ac transmission leads to a higher cable resistance, thereby increasing the thermal losses in the cable. The current rating of the cable is limited by the thermal losses per unit length of the cable that can be effectively dissipated to maintain the operating temperature at 90 °C. Therefore, for dissipating the same cable losses for maintaining the operating temperature at 90 °C, greater rated current can be drawn at sending end of the system as described by (5).

$$I_{\text{dc,rated}} = \sqrt{\frac{I^2_{\text{ac,rated}}R_{\text{ac,90}}}{R_{\text{dc,90}}}} \tag{5}$$

where $R_{\text{ac,90}}$ and $R_{\text{dc,90}}$ are the cable resistance per unit length at 90°C operating temperature under ac and dc conditions. Fig. 3. depicts the capacity enhancement due to dielectric losses as well as absence of skin and magnetic proximity effect under dc conditions for varying cable conductor cross-sectional area.

2.2.3. Thermal Proximity

Enhancement in current carrying capacity of a cable due to its thermal proximity to other current carrying conductors is relevant specific to the system topology described in Section 2.4.2. Therein, three lines of ac system topology are refurbished to a balanced two line bipolar link with ground return or redundant line metallic return. Therefore, at full load rated cable current operation, conductive losses per unit length of the entire link are greater in ac case ($3 \times I^2_{\text{rated,ac}}R_{\text{ac,90}}$) as compared to dc ($2 \times I^2_{\text{rated,dc}}R_{\text{dc,90}}$). The three core cable current rating increase due to one redundant line in dc conditions can be estimated by incorporating a thermal proximity correction factor k_{tp} in (3) as given in (6).

$$I_{\text{dc,rated}} = k_{\text{tp}}\sqrt{\frac{I^2_{\text{ac,rated}}R_{\text{ac,90}}}{R_{\text{dc,90}}}} \tag{6}$$

k_{tp} is in the range of 1–1.5 depending on the ambient temperature and thermal properties of the conductor surrounding. Assuming uniform temperature around the cable and considering all three cores as single unit, the maximum value of k_{tp} is 1.5.

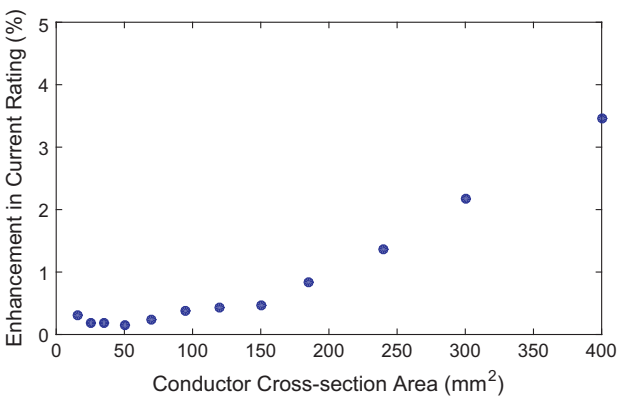

Fig. 3. Current rating enhancement in dc due to reduction of dielectric losses and absence of skin and magnetic proximity effects of ac operation.

2.2.4. Capacitive currents

When rated current is drawn from the sending end under ac conditions, a component of it is lost as leakage capacitive current and thereby reducing the delivered active power at the receiving end. The quantification is incorporated in the ac real power calculations in Section 2.1.

The capacity drop under ac conditions increases with higher cable cross-sectional area as the capacitance increases and is as much as ≈0.5% of the rated power for a 30 km link [17]. The relevance of capacitive effects increases with link length and operating voltage.

2.3. DC voltage capacity enhancement

2.3.1. Voltage regulation

In ac conditions, the frequency dependent voltage drop across the cable inductance and resistance results in the reduction of the receiving end voltage of the transmission line. This variation is called voltage regulation [24], which depends on the cable length, conductor cross-sectional area and also the load power factor. Under dc conditions, the inductive voltage drop is absent under steady state and the resistive drop is lower, thereby resulting in better voltage regulation. Roughly, 2–5% capacity enhancement can be achieved by operating under dc conditions for a 10 km cable link [9]. In Section 2.1, a precise mathematical representation of voltage regulation with varying link parameters and load power factors is quantified.

For ac transmission for longer distances, the capacity drop due to reactive components can be enhanced by employing voltage regulators at specified distances. However, experts from distribution network operators (DNOs) advice that for applications with short distances as considered in this paper, the price and operating losses of voltage regulator may render its installation non-viable.

2.3.2. Voltage imposed on cable insulation

In ac, a peak voltage of $\sqrt{2}$ times the rms appears twice per cycle across the cable insulation. Apart from bearing the peak fields per cycle in ac transmission, the switching transients are much worse than in dc [25]. It should also be noted that the three phase ac lines are generally chosen with insulation that can continuously bear $\sqrt{3}V_{\text{n}}$, where V_{n} is the nominal voltage. This factor of $\sqrt{3}$ can appear across the healthy phases for a significant period of time when single line to ground fault occurs. Such issues are not prevalent in dc conditions.

Considering the above aspects, it is possible to raise the rated operating voltage imposed on the cables under dc conditions at least by a factor of $\sqrt{2}$ corresponding to the peak ac voltage [26]. The technical consequences of this enhancement of cable operating

voltage rating on the insulation under dc conditions is discussed in Section 4.

2.4. Quantified capacity enhancement for different system topologies

In this section, the complete quantized capacity results will be presented for different ac and dc system configurations. All the factors discussed in the preceding sections will be mathematically incorporated. The existing ac system topology and the final dc system topology can influence the achieved enhancement in capacity. In fact, in some scenarios, this can even lead to reduced capacity in the final system despite operational benefits of dc system.

The dc system can either be a monopolar link with ground return or a bipolar link. The receiving end power for a single monopolar dc link with ground return $P_{r,mp}$ and a single bipolar link $P_{r,bp}$ is given by (7) and (8) respectively.

$$P_{r,mp} = I_{s,dc}^2\left(\frac{V_{s,dc}}{I_{s,dc}} - (L \times R_{dc,90} + R_{gnd})\right) \quad (7)$$

$$P_{r,bp} = I_{s,dc}^2\left(\frac{2V_{s,dc}}{I_{s,dc}} - (2L \times R_{dc,90})\right) \quad (8)$$

where $I_{s,dc}$ and $V_{s,dc}$ are the sending end current and voltages respectively, equal to the rated values for the cable of length L in km under dc operating conditions. $R_{dc,90}$ is the dc cable resistance in Ω/km at operating temperature of 90 °C and R_{gnd} is the ground resistance assumed to be designed at 0.5 Ω.

2.4.1. 3-phase single circuit ac to monopolar dc link

Fig. 4a. depicts the refurbishment of a single circuit three core underground cable connecting 3 phase ac substations at either side to operate as a monopolar dc link with ground return. It must be ascertained that ground return is permissible in the area of installation as it can lead to corrosion and damage to underground metallic structures.

The system can be designed for modularity and greater reliability by having 3 links with two converters for each link at sending and receiving end. However, as shown in this figure, the three cores can also be connected to form a single link between two converters with three times the power capacity. This choice is a trade-off to achieve higher efficiency and lower cost instead of greater modularity. The percentage capacity enhancement $CE_{mp,3l}$ is given by (9).

$$CE_{mp,3l} = \left(\frac{3P_{r,mp} - 3P_{r,ac}}{3P_{r,ac}}\right) \times 100 \quad (9)$$

Fig. 4b depicts the total power transfer capacity enhancement for different cable conductor cross-sectional areas and link lengths for unity load power factor. Most of the enhancement (about 40%) comes from higher dc voltage rating of $\sqrt{2}$ times $V_{ac,rms}$. Better voltage regulation is another influencing factor, particularly for lower area of cross-sections and longer link lengths. Capacity enhancement due to skin and proximity effect and dielectric losses is discernible for higher conductor areas.

2.4.2. 3-phase single circuit ac to 1× bipolar dc link

The system is depicted in Fig. 5a. Out of the three cores of the ac cable, two are used for full power transfer in a bipolar dc topology. The third line shown in dash is redundant or supports ground return which carries negligible current under balanced conditions. Also it can be used during faults, where the system topology can be swapped to monopolar operation with 50% of the bipolar loading [25].

The percentage capacity enhancement $CE_{bp,3l}$ is given by (10).

$$CE_{bp,3l} = \left(\frac{P_{r,bp} - 3P_{r,ac}}{3P_{r,ac}}\right) \times 100 \quad (10)$$

Fig. 5b shows the capacity enhancement results for different conductor cross-sectional area and cable length for unity load power factor. The power transferred to receiving end by the dc system is lower than its ac counterpart in some circuit configurations despite higher rated operating voltage, current and voltage regulation. This is because one conductor is unused during bipolar operation.

In this specific case, additional capacity gains over the ones depicted in Fig. 5b can be achieve due to the influence of thermal proximity which is described in Section 2.2.3.

2.4.3. 3-phase double circuit ac to 3× bipolar dc links

Fig. 6a shows the refurbishment of 3 phase double circuit ac cable to 3× bipolar dc links. The three cores of each cable are interconnected to form a bipolar link between four voltage source converters. Each converter is rated for half of the full load capacity of the power delivered to the ac side. The ground return carries negligible current under balanced operation. During faults, the system can operate as monopolar link with ground return at 50% of the rated capacity. However, it maybe possible only for short period of time at locations where corrosion due to ground current is not permissible.

Another possibility is to create three separate dc links with their own converter systems. The number of switches will triple but their current rating can be reduced. Since the cost and efficiency is more intimately tied with voltage rating and number of switches, this is a trade-off for the added modularity achieved in case a dc link fails. The capacity enhancement is the same, so this topic is not further explored in this paper.

The percentage capacity enhancement $CE_{bp,6l}$ is given by (11). In Fig. 6b, the capacity enhancement quantification is offered for

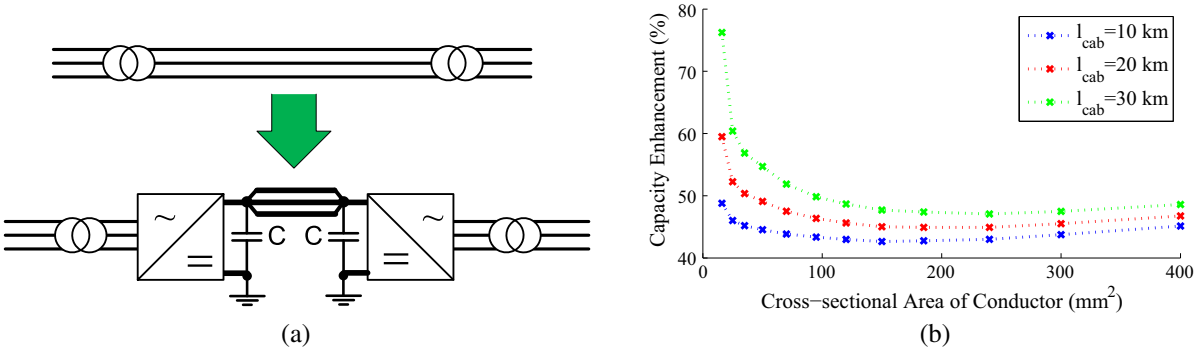

Fig. 4. Transmitted power capacity enhancement with conductor cross-sectional area for different cable lengths at unity load power factor for 3-phase single circuit ac to monopolar dc link with ground return.

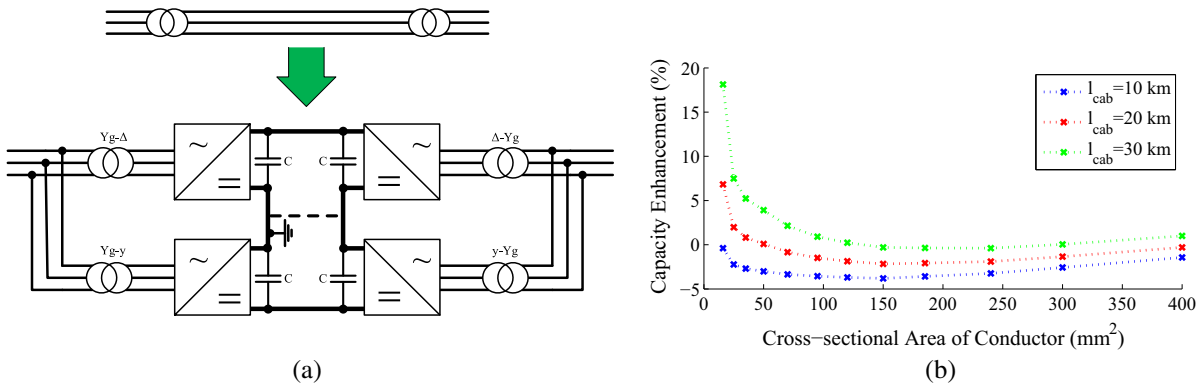

Fig. 5. Transmitted power capacity enhancement with conductor cross-sectional area for different cable lengths at unity load power factor for 3-phase single circuit ac to 1× bipolar dc links.

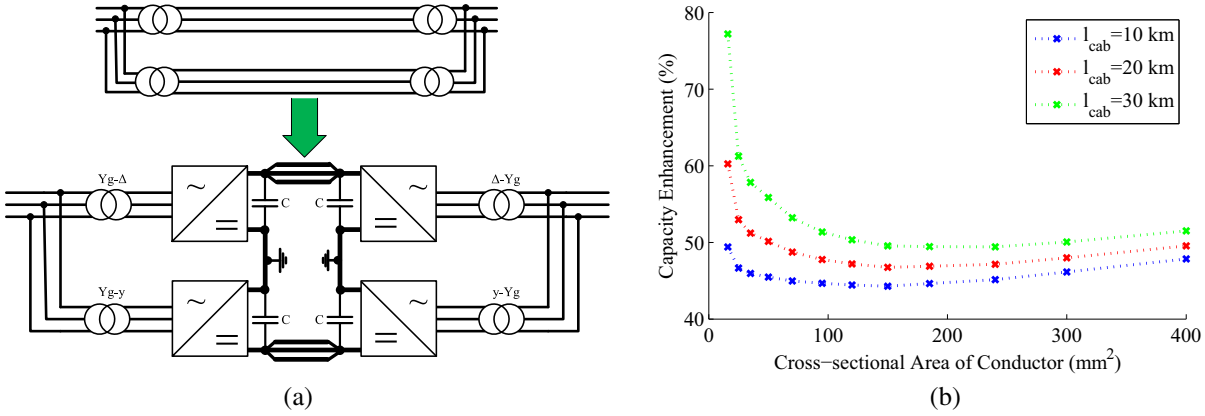

Fig. 6. Transmitted power capacity enhancement with conductor cross-sectional area for different cable lengths at unity load power factor for 3-phase double circuit ac to 3× bipolar dc links.

varying link length and conductor cross-sectional areas at unity load power factor.

$$CE_{\mathrm{bp,6l}} = \left(\frac{3P_{\mathrm{r,bp}} - 6P_{\mathrm{r,ac}}}{6P_{\mathrm{r,ac}}}\right) \times 100 \tag{11}$$

The trends in the percentage capacity enhancement presented in this section for all three system refurbishments can be explained as follows:

- With increasing cable length, the voltage regulation in ac system decreases due to increasing resistance and inductance. In dc, only the cable resistance increases, so the decrease in receiving end real ac power $P_{\mathrm{r,ac}}$ is greater than the decrease in receiving end dc power $P_{\mathrm{r,dc}}$. Therefore, the percentage capacity enhancement increases.
- With increasing conductor cross-sectional area the capacity enhancement is influenced in two ways:
  - The cable resistance and inductance decrease, leading to a better voltage regulation and higher receiving end real ac power. Fig. 2. shows that this impact is more prominent for lower areas, leading to higher capacity enhancement.
  - Impact of skin effect leads to higher capacity enhancement, which is more prominent for greater conductor area.

The opposing influence of these two factors leads to the profile of percentage capacity enhancement with respect to the cross-sectional area of the cable conductor.

2.5. Dependence on load power factor

Previous section describes the capacity enhancement considering that the receiving end ac load is operating at unity power factor. Substations employ power factor correction with passive capacitors in order to improve the power quality in ac distribution networks. These are cheap and robust devices requiring little maintenance. However, changing reactive power demand of the grid can only be met by stepped switching of relevant capacitor banks. Therefore, the average load power factor of the receiving end substation can be typically between 0.9 and 1.

With power electronic converters at both ends of the dc link, this reactive power demand can be met rapidly and smoothly and the cable only transmits the real power demand of the receiving end ac grid. Fig. 7 shows the additional percentage capacity enhancement factor (CEF) considering 0.9 load power factor.

10–20% additional capacity enhancement can be achieved in real power delivery to the receiving end of the distribution grid at 0.9 power factor. For case (b), the power factor dependent enhancement is also lower due to redundant line operation.

Part of the capacity enhancement is due to the direct dependence of the delivered real power on the load power factor. However, a non-linear enhancement can be observed with the link length and the conductor cross-sectional area due to the variation in voltage regulation with the load power factor. This is clearly noticeable in the quantified breakup of the various contributing factors in capacity enhancement for different cable cross-sectional areas is presented in Fig. 8. The topology is 3× bipolar

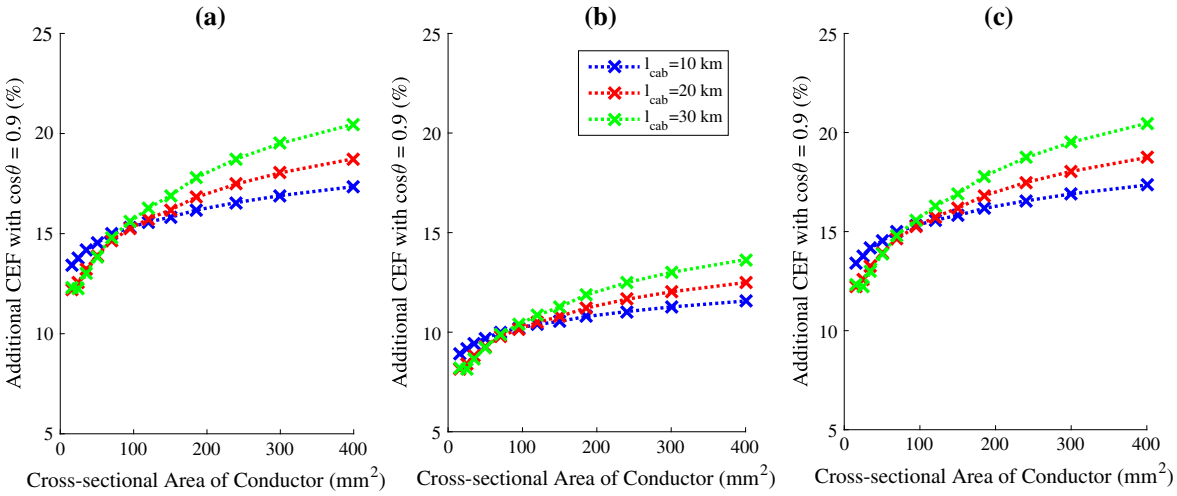

Fig. 7. Additional capacity enhancement for different conductor cross-sectional area for different cable lengths at 0.9 load power factor for (a) 3-phase single circuit ac to monopolar dc link with ground return (b) 3-phase single circuit ac to bipolar dc link (c) 3-phase double circuit ac to bipolar dc link.

links from 3-phase 3 line double circuit medium voltage ac cable link.

In Fig. 8, it can be observed that with lower power factor, the voltage regulation improves for lower cross-sectional area and worsens for higher areas for the same link length, which is reflected in the non linear profile of additional capacity enhancement of Fig. 7.

Fig. 8 summarizes the quantification of capacity enhancement for case (c) which is found to be most favourable from operational point of view as the ground currents are limited during normal operation. Monopolar refurbishment of case (a) offers similar enhancement but maybe unfavourable in some locations due to high ground currents. A realistic capacity enhancement of 50–60% can be achieved by refurbishing medium voltage ac underground cable to operate under dc conditions with the bulk of enhancement coming from voltage rating increase (41%), followed by load power factor (10%), capacitive currents and voltage regulation 5–10%. Current rating increase due to skin and

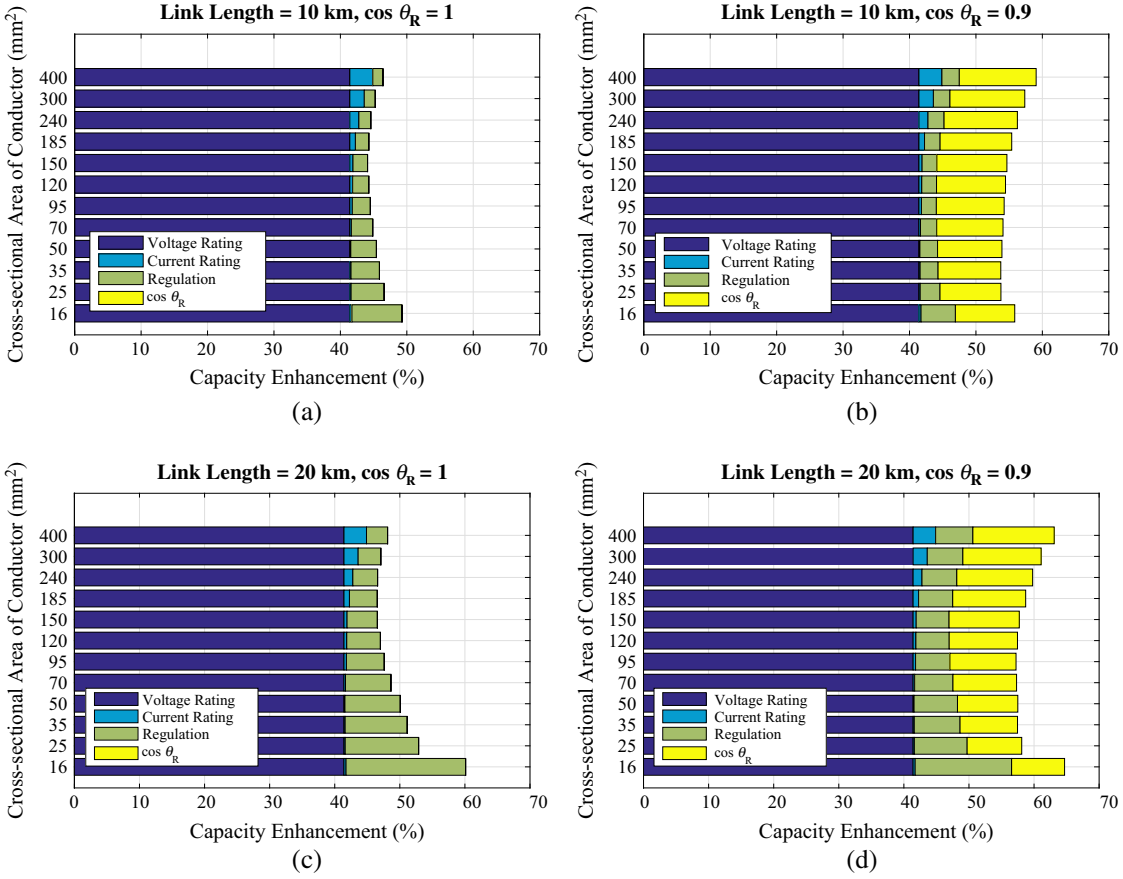

Fig. 8. Factor split of capacity enhancement by refurbishing 3 phase double circuit ac cable link to 3× bopolar dc link.

proximity effect as well as dielectric losses are relevant contributing factors for higher conductor cross-sectional areas.

The capacity enhancement offers a business case for making use of the existing ac infrastructure under dc conditions when digging and laying cables is not a technically viable option. Additional costs of end converter systems can be balanced against the savings in digging, labour and copper costs. Further, the final system operating under dc is more efficient and provides energy savings, which is explored in the subsequent section.

3. System efficiency enhancement and its tradeoff with MMC station investment cost

Under dc operation, the cable efficiency improves but additional losses are incurred due to the converters. The net system level efficiency depends on the cable length, area of cross-section and the load power factor. From the context of the converter, the power rating determines the operating efficiency. The net system efficiency enhancement under specific viable configurations can be a trade-off for the higher incurred costs of converter substations.

3.1. Cable efficiency

All the factors that result in the capacity enhancement such as skin and proximity effect, dielectric losses, voltage enhancement, voltage regulation and load power factor also make dc cable operation more efficient as compared to ac. The derived equations in Appendix A are used to establish the efficiency enhancement ($\Delta\eta$) based on the identified factors.

The quantified results for efficiency enhancement ($\Delta\eta$) for the medium voltage ac cable link to operate under dc conditions for varying cable lengths cross-sectional areas and power factors are shown in Fig. 9. Herein, Case (a) is refurbishment from 3-phase 3 line single circuit ac system to 3× monopolar dc links with ground return, Case (b) is refurbishment from 3-phase 3 line single circuit ac system to 1× bipolar dc link and Case (c) is refurbishment from 3-phase 3 line double circuit ac system to 3× bipolar dc links.

The efficiency enhancement in Case (c) is the maximum as the per conductor sending end current drawn to supply the same power (rated per phase real power in ac system) is minimum. Case (a) has similar enhancement in efficiency, but slightly lower than Case (c) due to higher resistance of the ground return. In Case (b) the sending end current drawn per conductor is similar to the ac system, due to which the efficiency enhancement is lowest. However, due to reduced cable dc resistance and enhanced rated voltage, efficiency enhancement is still achieved in case (b).

As the cable length increases or the load power factor drops, the efficiency enhancement is higher. The variation in efficiency with conducted cross-sectional area is due to variation in resistance and also due to voltage regulation depending on the changing inductance and capacitance of the cable, such that the enhancement achieved is higher for lower cross-sectional area. Considering that the skin effect is dominant for larger areas, it can be concluded that the area dependence of the efficiency is largely governed by voltage regulation.

3.2. Converter efficiency

Converters are a very important part of the dc link. Although highly efficient, they add losses to the overall system, which need to be accounted for before drawing conclusions on the overall efficiency of the grid after the refurbishment of existing lines from ac to dc.

In dc links fast controllability and facilitation of bidirectional power flow is important, particularly at medium voltage distribution level. As a result, Voltage-Source Converters (VSC) are favored against Line-Commutated Converters (LCC) due to their inherent characteristics stemming from the use of IGBT switch valves. Furthermore, in LCC, bidirectionality is achieved with polarity reversal [9], which is inconsistent with XLPE cables due to the nature of fields it imposes. Therefore, VSC which achieves the same with current reversal, is favoured.

Recently, the focus of the research as well as of the main manufacturers is put on the development of Multi-level Modular Converters (MMC) due to several advantages over the conventional two-level VSC. More specifically, MMC offers reduced converter losses mainly because of the achieved drop in the operational switching frequency [27]. Moreover, MMC has higher robustness through the use of redundant submodules, as well as higher scalability due to the ease of construction. Another advantage is the smaller converter footprint, resulting in reduced mechanical requirements. Finally, the high ac-side current and voltage quality because of the high number of switching levels in the MMC results in low harmonics and thus, low ac filter requirements [28].

Taking these advantages into account, MMC are assumed in the dc grid terminals in this case study. To estimate the overall efficiency of the converter at different rated power levels, a fast MMC loss model was used, which captures the key sources of power losses in steady-state operation, as summarized below [29].

3.2.1. Conduction losses

The power dissipated by a IGBT and its antiparallel diode during one period is obtained according to:

$$\begin{cases} P_T = \frac{1}{T_f}\int_0^T K_{t,T}(V_{ce0}\cdot i_c + R_{ce0}\cdot i_c^2)dt \\ P_D = \frac{1}{T_f}\int_0^T K_{d,T}(V_{d0}\cdot i_d + R_{d0}\cdot i_d^2)dt \end{cases} \quad (12)$$

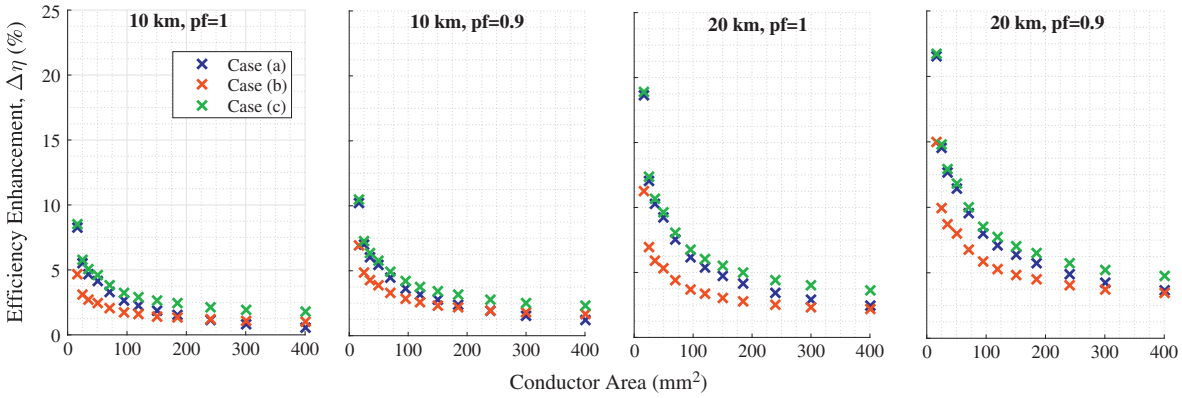

Fig. 9. Efficiency enhancement ($\Delta\eta$) for different cable cross-sectional areas, link lengths and load power factors.

where $K_{t,T}$ and $K_{d,T}$ are the datasheet temperature correction factors for the IGBT and diode, respectively, i_c and i_d are the collector and diode instantaneous currents, respectively, and T_f is the duration of one fundamental period.

3.2.2. Switching losses

The switching energy losses are calculated using the following expressions:

$$\begin{cases} E_{on} = E_{on,sheet}(I_{arm})k_{igbt,T,on}k_{igbt,R_G,on}k_{V_{dc}} \\ E_{off} = E_{off,sheet}(I_{arm})k_{igbt,T,off}k_{igbt,R_G,off}k_{V_{dc}} \\ E_{rec} = E_{rec,sheet}(I_{arm})k_{diode,T}k_{diode,R_G}k_{V_{dc}} \end{cases} \quad (13)$$

where E_{on}, E_{off} and E_{rec} are the IGBT's turn-on, turn-off and diode reverse recovery energies, respectively. The values of $E_{on,sheet}$, $E_{off,sheet}$ and $E_{rec,sheet}$ are obtained from the manufacturer's datasheet and further scaled with correction factors for temperature (k_T), gate resistance (k_{R_G}) and applied dc blocking voltage ($k_{V_{dc}}$).

3.2.3. Arm inductor losses

The ohmic losses of an arm inductor are given by:

$$P_{ind} = R^{\theta}_{ind} I^2_{arm,RMS} \quad (14)$$

where R^{θ}_{ind} is the ac (due to skin and proximity effects) and dc resistance of the arm inductor at θ°C and $I_{arm,RMS}$ is the RMS current of the MMC arm.

3.2.4. Cooling losses

The additional losses of the cooling system are added to the conduction, switching and inductors losses to obtain the total losses of the converter. Large converters usually make use of liquid cooling systems.

$$\begin{cases} P_{heat} = P_{con} + P_{sw} \\ P_{cool} = P_{heat} COP \end{cases} \quad (15)$$

where P_{heat} is the needs to dissipate, P_{con} is the total conduction losses, P_{sw} is the total switching losses, P_{cool} is the power demand of the cooling system and COP is the Coefficient of Performance of the cooling system. The COP is the ratio of the extracted heat over the power needed to achieve this extraction. In this work it is considered that COP = 20.

From the cable specifications, the nominal dc cable voltage and dc cable current were obtained for each of the twelve cases of cable conductor area considered in this study. Based on these values, the converter design was selected and the main MMC parameters for which the calculations were made are summarized in Table 1.

In the present study, the switches were selected based on the peak power rating considered hereby for the monopolar configuration, namely 8.7 MW. For lower power ratings, the converter is not optimally designed and thus, exhibits lower efficiency. Similarly, for the bipolar system, the converter is designed for a peak power of 26.1 MW.

As an example for the performed calculations, the losses breakdown and the efficiency of the MMC are presented in Fig. 10 for 300 mm^2 cable conductor area and converter power 7.7 MW. Similarly, the efficiency of the MMC was evaluated for all cable conductor areas and power ratings.

Table 1
MMC parameters.

MMC specifications	Unit	Value
Cell capacitance (C)	mF	4
Arm inductance (L)	mH	8
Number of SMs per arm (N)	–	30
Carrier frequency (f_c)	Hz	600

Fig. 10 (b) shows that the MMC can be optimized to have 99.34% efficiency at its rated power which does not vary much until 30–40% of its loading. Considering that there are 2 converters fully rated at the monopolar link (case (a)) cable power transfer capacity, while 4 converters of half the link capacity for bipolar topologies of case (b) and case (c), the net system level efficiency was computed after adjusting for the additional converter losses.

3.3. Payback time

Fig. 11 shows the payback time for different cases of system topologies considered in this paper. The additional cost of converter station is considered as 50 €/kW [30,8] against the energy saving of efficient system operation. The dc power link is assumed to operate at an average load corresponding to the full load of its corresponding ac link with the dutch electricity cost of 0.1 €/kW h.

Additional cost savings can be achieved from infrastructural investment costs of avoiding digging and installing new cables to enhance the power transfer capacity between two substations. However, these savings are system specific and depend on the fore-casted increase in demand. Incorporating these savings will improve on the economic viability based on the generalized payback time that is presented in this section.

4. Key technical considerations in refurbishing AC cables to operate under DC conditions

The preceding sections develop insight into the operational benefits of using the XLPE ac cables under dc conditions. It is important, however, to keep in mind the technical implications of such an operational refurbishment [9].

4.1. Insulation ageing aspects

Ageing of the insulation is directly associated with lifetime and breakdown of the cable [18]. A cable's lifetime depends on three fundamental aspects - thermal behaviour, the transients occurring during dynamic operation and the long term degradation due to the steady state fields imposed on the insulation [31,32]. Interaction of these factors ultimately translate to mechanical defects and treeing that leads to final breakdown over time.

4.1.1. Thermal aspects

Thermal degradation of insulation limits the current rating of the cable. The temperature of insulation near the conductor surface is the highest and depends on the surrounding thermal resistance, insulation thickness, ambient conditions and the loading profile [33,34]. While operating under dc, if it is ensured that the steady state losses are similar to ac operation, the thermal degradation aspects are assumed to also be similar.

However, thermal profile across the insulation does have a unique secondary effect under dc conditions, as it modifies the electric field profile. This will be further explored in Section 4.2.

4.1.2. Electrical aspects

The electric fields that appear across the cable insulation affect its lifetime, specifically through the phenomenon of treeing due to defects [18]. Such voids are unavoidable during manufacturing and tend to grow over time. The influence of partial discharges and their interaction with voids in insulation in the growth of trees is noted to be more of a high field phenomena expected to present a lesser degree of problem at medium voltage level [32]. Unlike ac operation however, the electric field distribution across cable insulation under dc conditions [35] can change with operating conditions such as temperature dependent field inversion and field

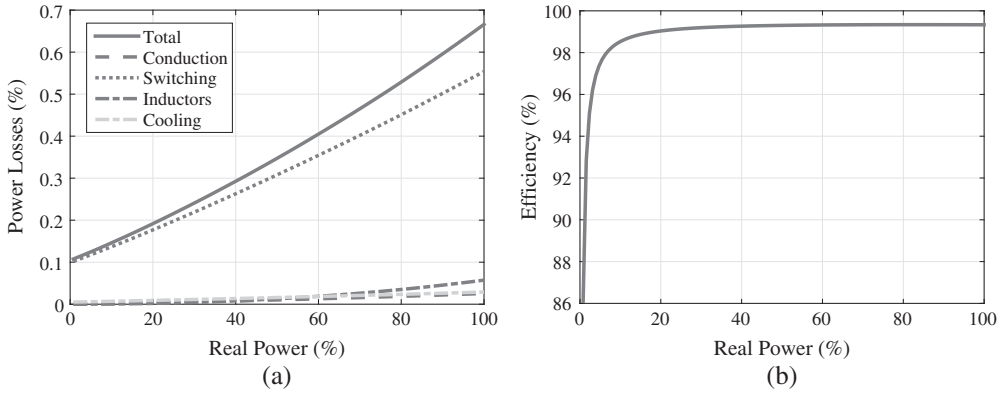

Fig. 10. Converter losses breakdown (a) and efficiency curve (b) for 300 mm^2 cable conductor area and converter power 7.7 MW.

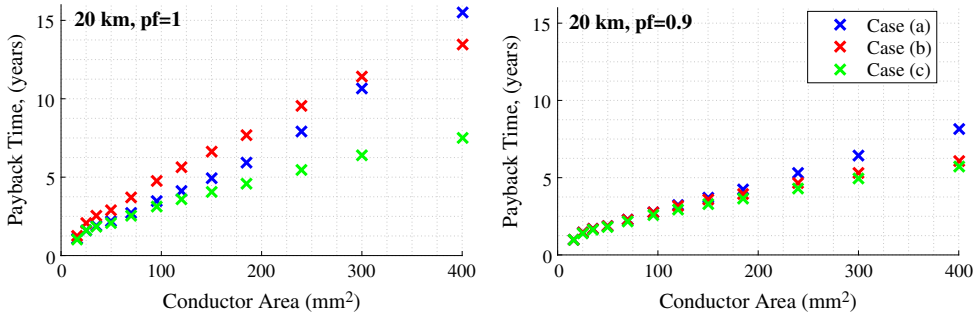

Fig. 11. Payback time based on energy savings due to system efficiency enhancement for different topologies.

enhancement due to polarity reversal. Also, the operational demands and therefore the transients occurring during dynamic operation and faults are different.

On a log–log scale the lifetime of insulation has an inverse linear relationship with the nominal electric fields for ac operation [31]. Under dc operating conditions, this relationship is not as clearly defined. Further, the steady state ac voltage profile cycles through a peak of $\sqrt{2}$ times the rms, a principle which is exploited to enhance the dc voltage for capacity and efficiency gains.

Since dc electric field is unidirectional in steady state, space charges are able to develop. While the effect of space charges is more prominent at high voltages, failure of polymeric cables due to these generally occurs due to polarity reversal or transient operation [32]. The Current Source Converter (CSC) achieves bi-directionality by polarity reversal [36], which imposes additional stress on the cable insulation. XLPE cables cannot perform well with polarity reversal [31], giving another reason for choosing voltage source based MMC in this study.

4.2. Temperature dependent dynamic line voltage rating

The electric field stress imposed due to operating dc voltage on the cable insulation exhibits temperature dependence [31,35], as the conductivity of the insulation changes with temperature. With increasing temperature and due to the fact that the dc electric field is unidirectional, space charges develop corresponding to the gradient in current density through the insulation that alter the field distribution.

4.2.1. Temperature dependent electric fields

The approximated expression for temperature dependent electric field stress E(x) on the cable insulation under dc operating conditions is given by (16) [31,35].

$$E(x) = \frac{\delta U_0 \left(\frac{x}{r_o}\right)^{(\delta-1)}}{r_o\left(1-\left(\frac{r_i}{r_o}\right)^{\delta}\right)} \tag{16}$$

U_0 is the nominal operating voltage imposed on the cable, r_i and r_o are the inner and outer radius of the insulation respectively and δ is a dimensionless quantity given by (17).

$$\delta = \frac{\frac{\alpha\Delta T}{\ln(r_o/r_i)} + \frac{bU_0}{r_0 - r_i}}{1 + \frac{bU_0}{r_0 - r_i}} \tag{17}$$

Herein, b is the stress coefficient in mm/kV, α is the temperature coefficient in °C^{-1} and ΔT is the temperature difference between outer and inner surfaces of the insulation.

4.2.2. Proposed novel concept – quantified illustration

Fig. 12 shows the resistive electric field distribution in the cable insulation for different ΔT for an example 11 kV single core XLPE cable [37] with $r_i = 11.28$ mm and $r_o = 14.68$ mm and $\alpha = 0.1$ °C, b = 0.03 mm/kV [31].

As the temperature difference increases, the electric field starts reducing at the inner insulation surface and increasing at the outer until it is completely inverted as observed in Fig. 12(a). It follows that at specific temperature distributions, it is possible to increase the operating voltage of the cable to obtain the same maximum field imposed on the insulation. Boundaries of the voltage rating enhancement must respect that the electric fields never become greater than the maximum field at the inner surface of the insulation at $\Delta T = 0$ °C.

4.2.3. Advantages of the proposed concept

Temperature dependent line rating by imposing a varying operating voltage on the cable while respecting the maximum electric

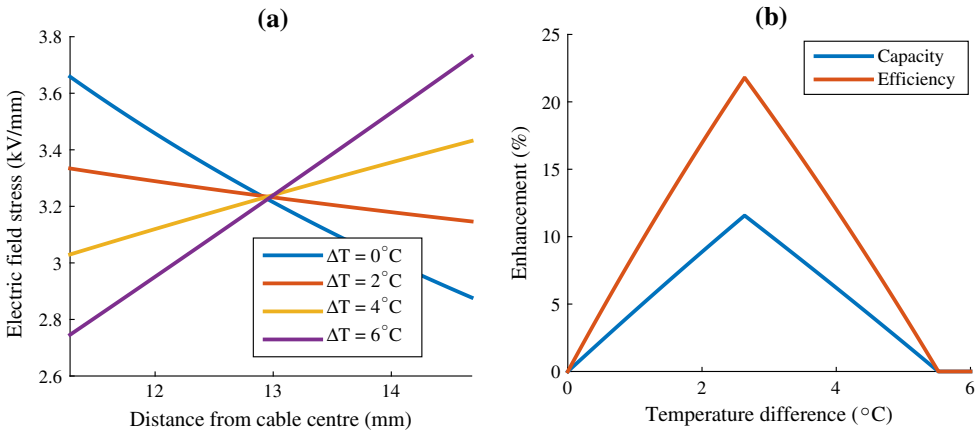

Fig. 12. Temperature dependence of (a) electric field stress on insulation of the cable (b) Transmission capacity and efficiency enhancement with proposed dynamic voltage rating.

field at any point in the insulation can have several advantages as highlighted below:

- Power transfer capacity boost is possible as a higher power can be transmitted for the same thermally defined current rating. Fig. 12(b) depicts the transmission capacity enhancement factor (CEF) in percentage. The algorithm used to compute the CEF is depicted in the flow diagram in Fig. 13.
  The algorithm is explained in the following steps:
  1. The electric fields are computed for the temperature difference (ΔT) between the inner and outer cable insulation surface from 0 °C to 6 °C in steps of 0.01 according to (16).
  2. The difference in electric field at the inner ($\Delta E(r_i)$) and outer ($\Delta E(r_o)$) insulation surface for each temperature step with respect to the field at inner surface (E_{max}) at ΔT = 0 °C is computed.
  3. The transmission capacity enhancement factor by which the voltage rating of the cable can be increased with temperature without breaching the maximum electric field (E_{max}) at any point of the insulation is computed.
- For the same transmitted power, an enhancement in voltage can lead to reduction in cable current by the same factor, leading to an enhancement in efficiency by a factor ($\Delta\eta$) given by (18),

$$\Delta\eta = \left(1 - \left(1 - \frac{CEF}{100}\right)^2\right) * 100 \tag{18}$$

  Enhancement in transmission efficiency with ΔT is also depicted in Fig. 12(b);
- Greater rate of change of active power $\frac{dP}{dt}$ can be injected into the grid by the inverter of the dc link. This is possible because $\frac{dP}{dt}$ is proportional to the dc link voltage [38].

4.2.4. Limitations

Specifically from the context of application of the proposed concept of temperature dependent dynamic voltage rating of the cable, the challenges are highlighted below:

- An estimate of the insulation temperature difference must be obtained from the cable current. For this purpose, a finite element method based thermal model of the underground cable

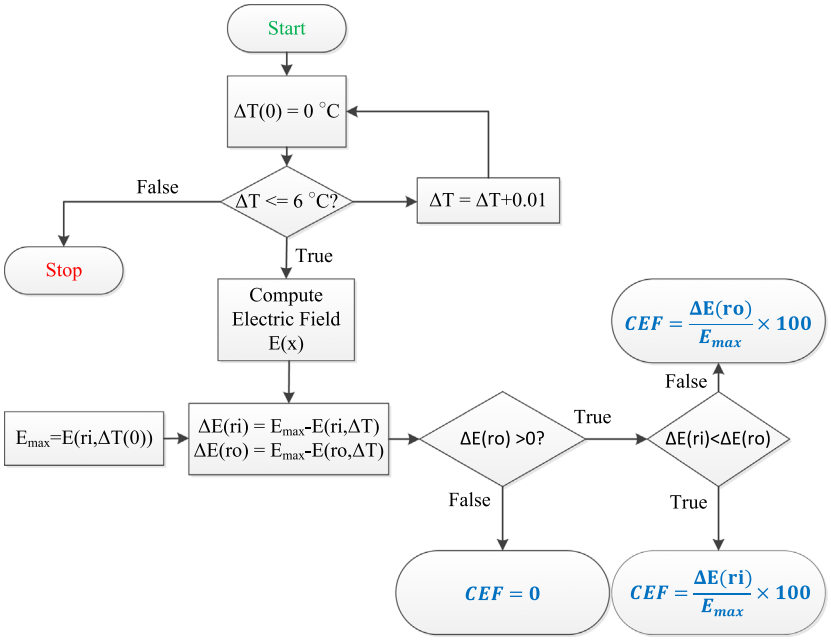

Fig. 13. Algorithm flowchart for computing the capacity enhancement factor (CEF).

must be developed. Thereby, realistic boundaries of expected temperature differences based on the cable current, ground temperature and insulation material must be obtained.
- The electrical time constant is generally much lower than the thermal. Therefore, the delay in temperature evolution in cable with expected variation in load current must be accounted for.
- The space charge accumulation is also time dependent, so the steady state electric fields may take minutes to hours to reach the described distribution.
- The set limit to which voltage can be enhanced has to be stringent taking into account that only a rough estimate of the insulation temperature can be obtained from the cable current measurements.
- The impact of temperature dependent voltage enhancement algorithm on the reliability of the system must be explored.
- Cable joints and the dc link converters must be over-designed to handle the higher voltages imposed on the cable. The trade-off in higher incurred costs against the enhancement in efficiency and transmission capacity must be considered.

Therefore, the translation of this concept to field level application is not so straightforward. However, it should also be noted that a small increase in voltage for a short while may not be significantly detrimental to the lifetime performance of insulation. The redundant sub-modules of the MMC may be used to achieve the dynamic voltage rating proposed in this paper.

5. Conclusions

By refurbishing the underground cable infrastructure to operate under dc conditions, costs of digging and laying new infrastructure can be avoided, while achieving significant capacity and efficiency gains. This is particularly advantageous for old heritage cities like Amsterdam, where digging can be not only expensive, but also difficult. Therefore, the benefit is socio-economic. The following technical insights can be derived from this paper:

- The computed results proved that a capacity enhancement of 50–60% can be achieved. A generalized trend was developed using mathematically sound, novel equations taking into account all relevant influencing factors. This can be extrapolated to help the utility grid operators decide how much gains can be achieved for their particular system by using the proposed novel concept.
- It was shown that the corresponding cable efficiency enhancement was 3–10% with a payback of about 5 years against added converter costs and losses. With the computed optimized MMC efficiency of 99.34% per substation converter at its rated power, the overall system efficiency was quantified and the corresponding payback trend based on the savings due to efficient operation was presented for all the studied cases.
- It was highlighted how the system topology could be important for making an techno-economically viable choice. For instance, it was found that 3-phase 3-line double circuit ac link refurbished to 3× bipolar link presented the maximum efficiency and lowest payback time. The capacity gains were similar to 3× monopolar link but bipolar topology was preferred due to the absence of corrosive effect of large ground currents.
- Insights were offered on the consequences of applying the proposed method on the XLPE cable insulation. Differences in the imposed electric fields were discussed.
- A novel concept of dynamic voltage rating was explored to provide an additional capacity enhancement of 10% and efficiency enhancement of 20%. The future challenges involved in implementing the concept were listed.

Acknowledgements

This work is funded by tki switch2smartgrids under the project Flexible and Future Power Links for Smart Grids for Rijksdienst voor Ondernemend, Nederland. We thank all the project partners for their involvement. Specifically, we would like to thank Maarten Van Riet from Alliander for helping us identify the critical grid location where issue of capacity enhancement is relevant.

Appendix A. Imposing rated current at sending end of the link

The equivalent circuit for underground MVAC cable link for power transmission described as a π-network is shown in Fig. A.14.

The reference phasor is the sending end voltage with magnitude corresponding to the cable operating voltage rating. The cable current rating is to be imposed as the sending end current magnitude with unknown angle θ_S depending on the cable parameters and the load impedance.

The cable parameters Z and Y can be computed in terms of the resistance (R_{cab}), inductance (L_{cab}) and capacitance (C_{cab}) based on the varying link length and conductor cross-section area.

In order to determine the receiving end real power $P_R = \text{real}(\vec{V}_R \cdot \vec{I}_R^*)$ for load power factor $\cos\theta_R$ varying from 0 to 1, the unknown sending end current angle θ_S and the load impedance magnitude $|Z_L|$ must be computed for varying cable lengths and conductor cross-sectional areas, such that, the rated cable current is drawn from the sending end.

The π-network of Fig. A.14. can be represented as a 2-port network with ABCD parameters [24] given by (A.1)–(A.4).

$$A = |A|\angle\alpha = 1 + \frac{YZ}{2} \tag{A.1}$$

$$B = |B|\angle\beta = Z \tag{A.2}$$

$$C = |C|\angle\gamma = Y\left(1 + \frac{YZ}{4}\right) \tag{A.3}$$

$$D = |D|\angle\delta = A \tag{A.4}$$

The receiving end voltage $\vec{V}_R$ and current $\vec{I}_R$ of this 2-port network are expressed in terms of the sending end parameters [39] by (A.5) and (A.6) respectively.

$$\vec{V}_R = D\vec{V}_S - B\vec{I}_S \tag{A.5}$$

$$\vec{I}_R = -C\vec{V}_S + A\vec{I}_S \tag{A.6}$$

The subsequent section deals with solving for the unknowns $|Z_L|$ and θ_S based on the above equations.

A.1. Computation of load impedance magnitude

The objective is to determine the load impedance magnitude $|Z_L|$ for varying cable length, conductor cross-sectional area and load power factor such that rated cable current $|I_S|$ is drawn from the sending end. The receiving end current can be expressed as,

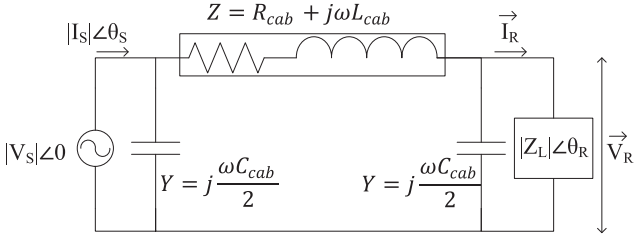

Fig. A.14. Equivalent circuit for underground MVAC distribution cable link.

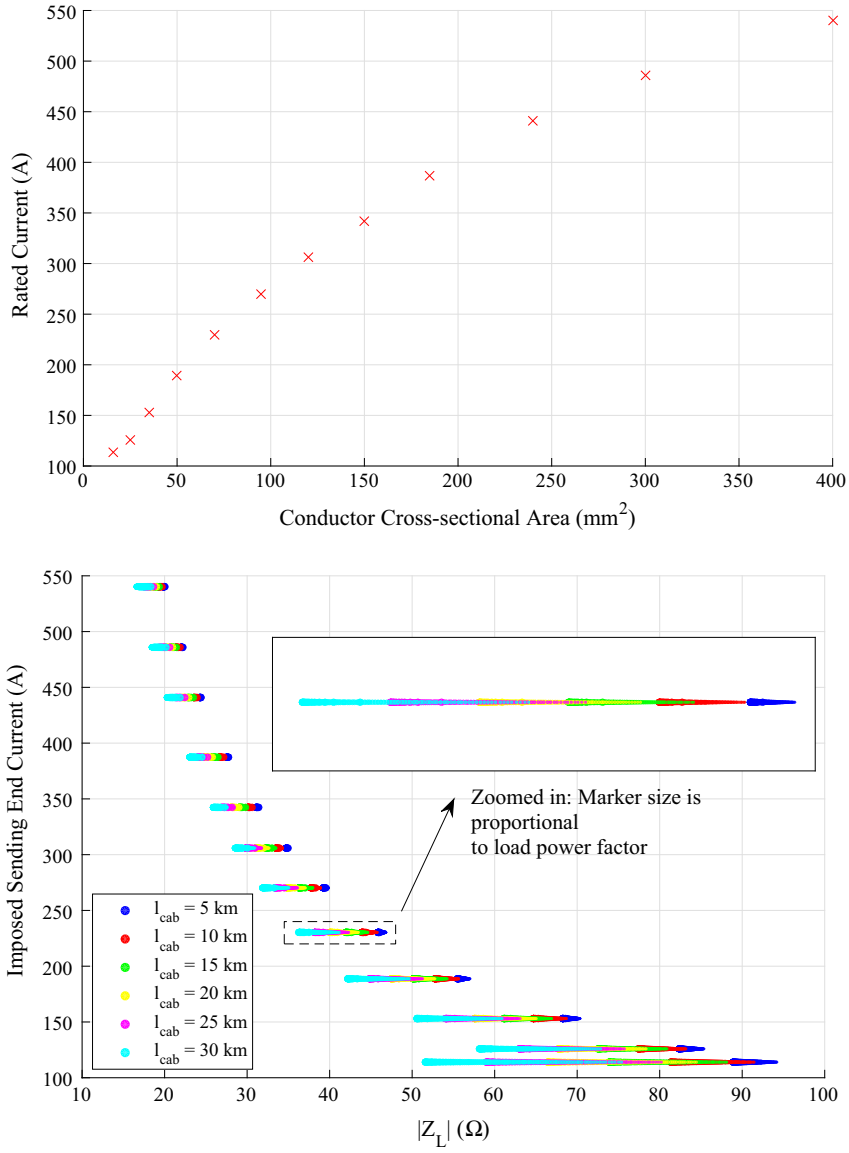

Fig. A.15. Computed load impedance magnitude with respect to imposed sending end cable current magnitude for varying cable lengths and load power factors.

Table B.2
Cable specifications as per datasheet [37].

A_{cond} (mm^2)	$I_{rated,gnd}$ (A)	$R_{dc,20}$ (Ω/km)	$R_{ac,90}$ (Ω/km)	L (mH/km)	C (μF/km)
16	114	1.15	1.47	0.45	0.2
25	126	0.727	0.927	0.39	0.22
35	153	0.524	0.668	0.37	0.24
50	189	0.387	0.493	0.35	0.27
70	230	0.268	0.342	0.34	0.3
95	270	0.193	0.247	0.32	0.34
120	306	0.153	0.196	0.31	0.37
150	342	0.124	0.159	0.30	0.40
185	387	0.0991	0.128	0.29	0.43
240	441	0.0754	0.0984	0.28	0.48
300	486	0.0601	0.0797	0.27	0.53
400	540	0.0470	0.0639	0.26	0.59

$$\vec{I_R} = \frac{\vec{V_R}}{|Z_L|\angle\theta_R} \tag{A.7}$$

Substituting (A.7) in (A.6) and solving for $\vec{I_S}$ using (A.5), we obtain,

$$\vec{I_S} = \left(\frac{D + C\cdot(|Z_L|\angle\theta_R)}{B + A\cdot(|Z_L|\angle\theta_R)}\right)\vec{V_S} \tag{A.8}$$

Separating and equating the real and imaginary parts of (A.8),

$$\begin{aligned}&|V_S|(|D|\cos\delta + |C||Z_L|\cos(\gamma+\theta_R)\\ &= |I_S|\cos\theta_S(|B|\cos\beta + |A||Z_L|\cos(\alpha+\theta_R)\\ &\quad - I_S|\sin\theta_S(|B|\sin\beta + |A||Z_L|\sin(\alpha+\theta_R)\end{aligned} \tag{A.9}$$

$$\begin{aligned}&|V_S|(|D|\sin\delta + |C||Z_L|\sin(\gamma+\theta_R)\\ &= |I_S|\cos\theta_S(|B|\sin\beta + |A||Z_L|\sin(\alpha+\theta_R)\\ &\quad + I_S|\sin\theta_S(|B|\cos\beta + |A||Z_L|\cos(\alpha+\theta_R)\end{aligned} \tag{A.10}$$

Rearranging both (A.9) and (A.10) to express $|Z_L|$ in terms of θ_S,

$$|Z_L| = \frac{|V_S||D|\cos\delta - |I_S||B|\cos(\beta+\theta_S)}{|I_S||A|\cos(\theta_S+\theta_R+\alpha) - |V_S||C|\cos(\theta_R+\gamma)} \tag{A.11}$$

$$|Z_L| = \frac{|V_S||D|\sin\delta - |I_S||B|\sin(\beta+\theta_S)}{|I_S||A|\sin(\theta_S+\theta_R+\alpha) - |V_S||C|\sin(\theta_R+\gamma)} \tag{A.12}$$

We have two equations for two unknowns ($|Z_L|$ and θ_S). Equating (A.11) and (A.12) and simplifying, θ_S is given by (A.13).

$$x\sin\theta_S + y\cos\theta_S = \lambda \tag{A.13}$$

Herein, x, y and λ are known from the line parameters varying based on the cable length, conductor cross-section area and the load power factor, given by the expressions,

$$x = |A||D|\cos(\alpha+\theta_R-\delta) - |B||C|\cos(\beta-\theta_R-\gamma) \tag{A.14}$$

$$y = |A||D|\sin(\alpha+\theta_R-\delta) - |B||C|\sin(\beta-\theta_R-\gamma) \tag{A.15}$$

$$\lambda = \frac{|V_S|^2|C||D|\sin(\gamma+\theta_R-\delta)}{|V_S||I_S|} + \frac{|I_S|^2|A||B|\sin(\alpha+\theta_R-\beta)}{|V_S||I_S|} \tag{A.16}$$

Thereby, the solution of (A.13) for θ_S is given by (A.17),

$$\theta_S = \sin^{-1}\left(\frac{\lambda}{\sqrt{x^2+y^2}}\right) - \tan^{-1}\left(\frac{y}{x}\right) \tag{A.17}$$

Therefore, the magnitude of load impedance $|Z_L|$ for imposing the rated cable current at the sending end of the MV distribution line can be computed by substituting the value of θ_S found from (A.17) in (A.11) and/or (A.12).

A family of load impedance magnitudes $|Z_L|$ are obtained, that would impose the rated cable current at the sending end for different cable lengths from 5 to 30 km in steps of 5 km, conductor cross-section of 16 to 400 mm^2 and load power factor varying from 0 to 1 in steps of 0.01. as shown in Fig. A.15.

It can be observed that the actual imposed sending end cable current magnitude is equal to the current rating for the conductor cross-sectional area in the specified circuit configuration.

- The marker size is proportional to the load power factor.
- As the cable length increases, the magnitude of $|Z_L|$ required to impose the rated cable current at sending end decreases.

Using the computed magnitude of $|Z_L|$ for all 7272 circuit configurations and the phase angle θ_S to impose the rated cable current at sending end, with rated sending end voltage as the reference phaser, the receiving end voltage and current can be determined using (A.5) and (A.6) respectively.

Finally, the transmitted real power at the receiving end can be computed from (A.18).

$$P_R = real(\vec{V_R}.\vec{I_R}^*) \tag{A.18}$$

Appendix B. Cable parameters

The computation results presented in this paper are for a 3-core 11 kV armoured XLPE insulated medium voltage cable with copper conductor. Nameplate specifications [37] for cable parameters are presented in Table B.2.

References

[1] Paterakis NG, Gibescu M. A methodology to generate power profiles of electric vehicle parking lots under different operational strategies. Appl Energy 2016;173:111–23. http://dx.doi.org/10.1016/j.apenergy.2016.04.024, <http://www.sciencedirect.com/science/article/pii/S0306261916304743>.

[2] Silvester S, Beella SK, van Timmeren A, Bauer P, Quist J, van Dijk S. Exploring design scenarios for large-scale implementation of electric vehicles; the Amsterdam Airport Schiphol case. J Cleaner Prod 2013;48:211–9. environmental Management for Sustainable Universities (EMSU) 2010European Roundtable of Sustainable Consumption and Production (ERSCP) 2010.

[3] Capasso C, Veneri O. Experimental study of a {DC} charging station for full electric and plug in hybrid vehicles. Appl Energy 2015;152:131–42. http://dx.doi.org/10.1016/j.apenergy.2015.04.040, <http://www.sciencedirect.com/science/article/pii/S030626191500495X>.

[4] Mouli GC, Bauer P, Zeman M. System design for a solar powered electric vehicle charging station for workplaces. Appl Energy 2016;168:434–43.

[5] Gustafsson M, Gustafsson MS, Myhren JA, Bales C, Holmberg S. Techno-economic analysis of energy renovation measures for a district heated multi-family house. Appl Energy 2016;177:108–16. http://dx.doi.org/10.1016/j.apenergy.2016.05.104, <http://www.sciencedirect.com/science/article/pii/S0306261916307061>.

[6] Rogers J, Cooper S, Grady O, McManus M, Howard H, Hammond G. The 20% house – an integrated assessment of options for reducing net carbon emissions from existing {UK} houses. Appl Energy 2015;138:108–20. http://dx.doi.org/10.1016/j.apenergy.2014.10.047, <http://www.sciencedirect.com/science/article/pii/S0306261914010976>.

[7] Schiphol deploys 35 electric buses. <https://www.schiphol.nl/SchipholGroup/NewsMedia/PressreleaseItem/SchipholDeploys35ElectricBuses.htm> [accessed: 2016-09-01].

[8] Shekhar A, Prasanth V, Bauer P, Bolech M. Economic viability study of an on-road wireless charging system with a generic driving range estimation method. Energies 2016;9(2):76. http://dx.doi.org/10.3390/en9020076, <http://www.mdpi.com/1996-1073/9/2/76>.

[9] Shekhar A, Kontos E, Mor AR, Ramírez-Elizondo L, Bauer P. Refurbishing existing MVAC distribution cables to operate under dc conditions. In: Power electronics and motion control (PEMC), 2016 IEEE 17th international conference and exposition on; 2016.

[10] Jovcic D, Ahmed K. High voltage direct current transmission: converters, systems and dc grids.

[11] Arrillaga J, Liu Y, Watson NR. Flexible power transmission. Wiley; 2007.

[12] Clerici A, Paris L, Danfors P. HVDC conversion of HVAC lines to provide substantial power upgrading. IEEE Trans Power Deliv 1991;6(1):324–33. http://dx.doi.org/10.1109/61.103755.

[13] Rahman H, Khan BH. Power upgrading of transmission line by combining ac–dc transmission. IEEE Trans Power Syst 2007;22(1):459–66. http://dx.doi.org/10.1109/TPWRS.2006.887895.

[14] Larruskain DM, Zamora I, Abarrategui O, Aginako Z. Conversion of {AC} distribution lines into {DC} lines to upgrade transmission capacity. Electr Power Syst Res 2011;81(7):1341–8. http://dx.doi.org/10.1016/j.epsr.2011.01.020, <http://www.sciencedirect.com/science/article/pii/S0378779611000320>.

[15] Larruskain DM, Zamora I, Abarrategui O, Iturregi A. VSC-HVDC configurations for converting {AC} distribution lines into {DC} lines. Int J Electr Power Energy Syst 2014;54:589–97. http://dx.doi.org/10.1016/j.ijepes.2013.08.005, <http://www.sciencedirect.com/science/article/pii/S0142061513003360>.

[16] Kontos E, Bauer P. Analytical model of MMC-based multi-terminal HVDC grid for normal and DC fault operation. In: 2016 IEEE 8th international power electronics and motion control conference (IPEMC-ECCE Asia); 2016. p. 3613–20. http://dx.doi.org/10.1109/IPEMC.2016.7512874.

[17] Shekhar A, Kontos E, Ramírez-Elizondo L, Mor AR, Bauer P. Power transfer computations for medium voltage ac link by imposing rated current at sending end. In: Power electronics and motion control (PEMC), 2016 IEEE 17th international conference and exposition on; 2016.

[18] Krueger F. Industrial high voltage; 1992.

[19] Tanaka T, Bulinski A, Castellon J, Frechette M, Gubanski S, Kindersberger J, et al. Dielectric properties of XLPE/SiO_2 nanocomposites based on CIGRE WG D1.24 cooperative test results. IEEE Trans Dielectr Electr Insul 2011;18(5):1482–517. http://dx.doi.org/10.1109/TDEI.2011.6032819.

[20] Kuschel M, Kalkner W. Dielectric response measurements in time and frequency domain of different XLPE homo- and copolymer insulated

medium voltage cables. IEE Proc Sci Meas Technol 1999;146(5):243–8. http://dx.doi.org/10.1049/ip-smt:19990470.
[21] Mecheri Y, Medjdoub A, Boubakeur A, Boujemâa S. Characterization of laboratory aged MV XLPE cables using dielectric losses factor measurements. In: Electrical sciences and technologies in Maghreb (CISTEM), 2014 international conference on; 2014. p. 1–4. http://dx.doi.org/10.1109/CISTEM.2014.7076950.
[22] Murakami Y, Nemoto M, Okuzumi S, Masuda S, Nagao M, Hozumi N, et al. Dc conduction and electrical breakdown of MGO/LDPE nanocomposite. IEEE Trans Dielectr Electr Insul 2008;15(1):33–9. http://dx.doi.org/10.1109/T-DEI.2008.4446734.
[23] Ogata S, Maekawa Y, Terashima K, Okiai R, Yoshida S, Yamanouchi H, et al. Study on the dielectric characteristics of DC XLPE cables. IEEE Trans Power Deliv 1990;5(3):1239–47. http://dx.doi.org/10.1109/61.57962.
[24] Stevenson WD. Elements of power system analysis. McGraw Hill; 1962.
[25] AC-microgrids versus dc-microgrids with distributed energy resources: a review. Renew Sustain Energy Rev 2013;24:387–405. http://dx.doi.org/10.1016/j.rser.2013.03.067.
[26] A. Shekhar et al., Electric cables in ships and cities - can higher dc voltage be imposed as compared to ac? Energy Open International Workshop; 2014.
[27] Tande JOG, Kvamsdal T, Muskulus M, Beddard A, Barnes M. 12th deep sea offshore wind R&D conference, EERA DeepWind'2015 modelling of MMC-HVDC systems an overview. Energy Procedia 2015;80:201–12. http://dx.doi.org/10.1016/j.egypro.2015.11.423, <http://www.sciencedirect.com/science/article/pii/S1876610215021554>.
[28] Zhang Y, Ravishankar J, Fletcher J, Li R, Han M. Review of modular multilevel converter based multi-terminal HVDC systems for offshore wind power transmission. Renew Sustain Energy Rev 2016;61:572–86. http://dx.doi.org/10.1016/j.rser.2016.01.108, <http://www.sciencedirect.com/science/article/pii/S1364032116001386>.
[29] Rodrigues S, Papadopoulos A, Kontos E, Todorcevic T, Bauer P. Steady-state loss model of half-bridge modular multilevel converters. IEEE Trans Ind Appl 2016;52(3):2415–25. http://dx.doi.org/10.1109/TIA.2016.2519510.
[30] Doncker RWD. Power electronic technologies for flexible dc distribution grids. In: 2014 international power electronics conference (IPEC-hiroshima 2014 – ECCE ASIA); 2014. p. 736–43. http://dx.doi.org/10.1109/IPEC.2014.6869670.
[31] Marzinotto M, Mazzanti G. Extruded cables for high-voltage direct-current transmission: advances in research and development; 2013.
[32] Hebner RE, Gattozzi AL, Pekarek SD. Performance assurance for DC cables for electric ships. In: 2015 IEEE electric ship technologies symposium, ESTS 2015 i; 2015. p. 343–8. http://dx.doi.org/10.1109/ESTS.2015.7157916.
[33] Neher JH, McGrath MH. The calculation of the temperature rise and load capability of cable systems. Trans Am Inst Electr Eng. Part III: Power Apparatus Syst 1957;76(3):752–64. http://dx.doi.org/10.1109/AIEEPAS.1957.4499653.
[34] Tanaka T. Aging of polymeric and composite insulating materials. aspects of interfacial performance in aging. IEEE Trans Dielectr Electr Insul 2002;9(5):704–16. http://dx.doi.org/10.1109/TDEI.2002.1038658.
[35] Jeroense M, Morshuis P. Electric fields in HVDC paper-insulated cables. IEEE Trans Dielectr Electr Insul 1998;5(2):225–36. http://dx.doi.org/10.1109/94.671940.
[36] Guerrero JM, Vasquez JC, Matas J, De Vicuña LG, Castilla M. Hierarchical control of droop-controlled AC and DC microgrids – a general approach toward standardization. IEEE Trans Industr Electron 2011;58(1):158–72. http://dx.doi.org/10.1109/TIE.2010.2066534.
[37] XLPE Insulated Cables. Specifications Catalogue. Tenaga Cable Industries (TCI).
[38] Yazdani A, Iravani R. Voltage-sourced converters in power systems - modeling, control, and applications; 2010.
[39] Wadhwa CL. Electrical power systems. Wiley; 1983.